ABSTRACT

STIFFNESS PREDICTIONS OF CARBON NANOTUBE REINFORCED TWO AND THREE-PHASE POLYMER COMPOSITES

By

Eric Neer

December 2015

Carbon nanotubes are a relatively new area of research which has gained significant attention in published literature. One reason for this interest is their use in multi-phase composites, specifically where they can enhance traditional polymer matrices. Many authors have attempted to adapt conventional micromechanical analyses reserved for microfibers to the nano scale. A review of these works is presented. In depth analysis is provided on one of these two phase (nanotube and matrix) models, the Anumandla-Gibson model, originally published in 2006. A discussion of its strengths and sensitivities is given, with numerical data to support the conclusions. It is extended to three-phase composites through the use of classical laminated plate theory. A literature survey is conducted to gather published two and three-phase experimental results for comparison. Two phase experimental results agree well with the present model, whereas three phase data was limited, but initial comparisons were promising.

STIFFNESS PREDICTIONS OF CARBON NANOTUBE REINFORCED TWO AND THREE-PHASE POLYMER COMPOSITES

A THESIS

Presented to the Department of Mechanical and Aerospace Engineering

California State University, Long Beach

In Partial Fulfillment

of the Requirements for the Degree

Master of Science in Aerospace Engineering

Committee Members:

Hsin-Piao Chen, Ph.D. (Chair)
Hsun Chen, Ph.D.
George Tzong, Ph.D.

College Designee:

Antonella Sciortino, Ph.D.

By Eric Neer

B.S., 2012, California State Polytechnic University, Pomona

December 2015

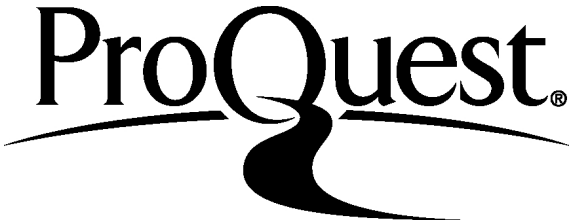

TABLE OF CONTENTS

Page

LIST OF TABLES

LIST OF FIGURES

FIGURE Page

CHAPTER 1

INTRODUCTION

Since their discovery in 1991, carbon nanotubes have been given considerable attention due to their exceptional stiffness, strength, and electrical properties. An ongoing area of research is investigating the nanotube's ability to serve as a reinforcement in conventional polymer matrices. Traditional unidirectional composite materials are known for their exceptional stiffness along the fiber direction, but suffer from poor out-of-plane properties. These off-axis properties are dominated by the matrix, and any enhancement to the matrix enhances these properties. Before nanotubes can be practically used however, we must have a way of estimating their stiffness contribution to see the degree of reinforcement they offer and if it is worth it.

Many "micromechanical" models exist for the prediction of microfiber lamina stiffness. Several authors have attempted to extend these models to the nano scale for nanocomposite analysis. Herein is presented a review of the current work done toward this goal, with an analysis of the benefits and drawbacks of each. Nanotube form is identified as an important parameter in stiffness predictions due to the sensitivity of nanotube modulus to geometry. In addition to the nanotubes' form, three other factors are discussed which are necessary for reliable nanocomposite stiffness predictions. These are nanotube dispersion in the matrix, orientation effects, and waviness effects.

The Anumandla-Gibson (A-G) model is a micromechanical framework which is chosen for detailed analysis, discussion of sensitivities, and comparison with published experimental results. The original model makes use of C.C. Chamis' micromechanical equations for analyzing a representative volume element (RVE)

consisting of matrix and nanotube. Since nanocomposites are generally fabricated at low nanotube volume fraction loadings, the A-G model is modified by replacing the Chamis equations with the Halpin-Tsai equations, which are known to agree well with experimental results of microfiber composites. Using classical laminated plate theory, the present model is then extended to the realm of so called "three-phase" composites which use microfibers and a matrix reinforced with carbon nanotubes. Again comparisons are made to the published experimental results. All of this is accomplished through development of a comprehensive MATLAB framework to test various combinations of fiber, matrix, and nanofiber in order to simulate experimental results.

Good agreement is seen between the original and modified models and two-phase experimental data. However, the modified A-G model offers a smaller range of possible waviness values, which is important for several reasons. Three-phase composite data is limited to one data-set, but initial results are promising given that the present model predicts experimental results for unidirectional and quasi-isotropic laminates to within a few percent.

CHAPTER 2

LITERATURE REVIEW

2.1 Properties of Carbon Nanotubes

2.1.1 Form

Carbon nano-reinforcements exist in several forms, most notably single-walled carbon nanotubes (SWNTs), multi-walled carbon nanotubes (MWNTs), and carbon nanofibers (or nanoropes). The basis for each of these forms is the single-walled nanotube, which is a rolled up graphene sheet composed of carbon in a planar hexagonal structure, like that shown in Figure 2.1 [1].

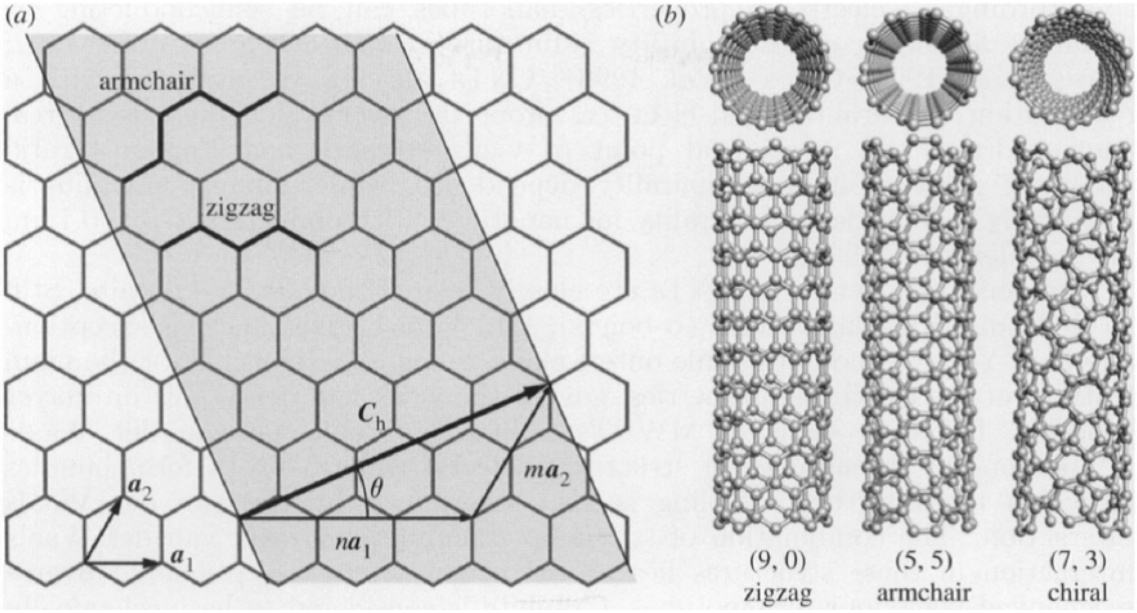

FIGURE 2.1. Single walled carbon nanotubes with varying chiral vectors. [2]

Different geometries of SWNTs can be made depending on the degrees of twist, which is described by the tube's "chiral" or "roll-up" vector, C_h, in the form (Pipes et al. [3]):

$$C_h = na_1 + ma_2 \tag{2.1}$$

where (n, m) are the integers shown in parenthesis in the right of the Figure 2.1. The case where $n > 0$ and $m = 0$ is termed "zigzag", $n = m$ is "armchair", and anything else is "chiral". A nanotube's roll up vector is significant in determining some of its properties (e.g. electrical conductance) and less so for others (e.g. stiffness). Gao et al. performed molecular dynamics simulations to investigate the effect of chirality on nanotube stiffness and found that for approximately equal nanotube diameters, stiffness was not a strong function of chirality [4]. With the focus of this study being on nanocomposite stiffness, chirality will not be considered.

Multi-walled nanotubes (Figure 2.2) consist of a series of concentric SWNTs and have diameters on the order of nanometers (depending on the number of SWNT layers) with possible lengths in excess of 1mm [5]. These length scales also apply to nanofibers (Figure 2.3), where instead of being concentric, SWNTs are bound tightly together in a crystalline array through Van der Waals forces [2]. Collectively, these and other tube forms will be referred to as carbon nanotubes, CNTs.

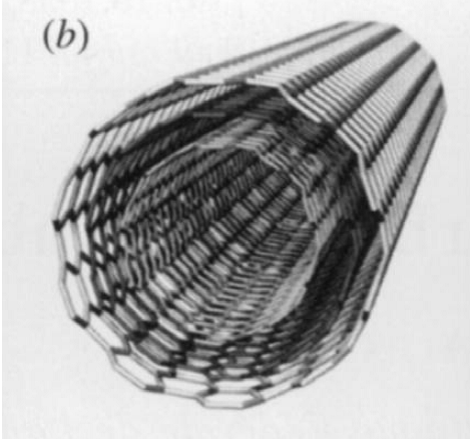

FIGURE 2.2. Multi-walled nanotube schematic. [2]

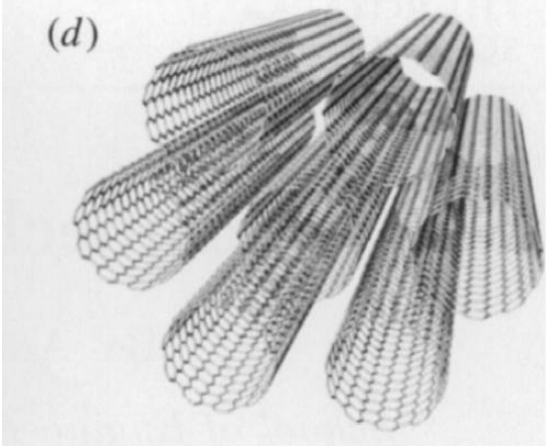

FIGURE 2.3. SWNT bundle (carbon nanofiber). [2]

2.1.2 Young's Modulus, Geometry, and Density

For simplicity's sake, it is tempting to assign a Young's Modulus to a nanotube form for use in a micromechanical model, as is done with conventional microfibers. To this end, several studies have attempted to predict an elastic modulus for carbon nanotubes, but have reported a wide range of values. For example, Lourie and

Wagner [6] give SWNT modulus values between 2.8 - 3.5 TPa and MWNT values between 1.7 - 2.4 TPa, whereas Sanchez et al. [7] and Yakobson and Avouris [8] report MWNT moduli being approximately 1 TPa and relatively independent of diameter. These and other large discrepancies are due in part to the authors treating nanotubes as they would a continuum, without careful consideration of their discrete nature.

Yakobson and Avouris [8] state that defining an elastic modulus implies a statistical spatial uniformity of the material. Since characteristic nanotube dimensions are on the same order as the dimensions of the carbon atoms that the tube is comprised of, there is a lack of "translational invariance" in the radial direction. Thus, a nanotube (whether SWNT, MWNT, or CNF) is not a *material*, but is more accurately an *engineering structure* [8]. Since CNTs must be treated as engineering structures, one cannot define an effective stiffness without taking into consideration the geometry of the CNT in question.

Pipes et al. [3] studied in-depth the intercorrelation between SWNT geometry, density, and tensile modulus by first considering the SWNT as a shell with thickness $\nu = 0.34nm$, the planar separation between layers in graphite. Figure 2.4 (a) depicts the shell model and also shows the carbon atoms comprising the shell. The midplane radius, R_n, of the shell is a function is a function the nanotube's chirality and the carbon-carbon bond length, 1.421 Å [9]. With this information, the cross sectional area of the open cylinder can now be defined. This area is then assigned a modulus $E_n = 1029GPa$, the in-plane modulus of graphite.

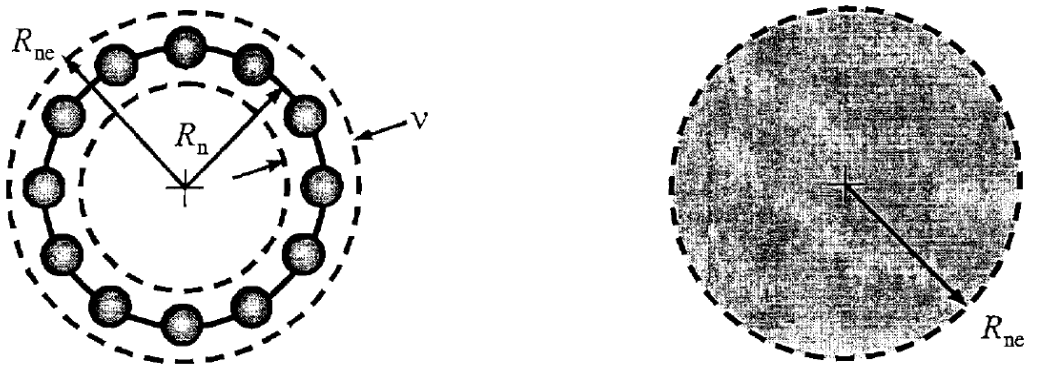

FIGURE 2.4. SWNT and equivalent filled cylinder. [3]

The product of area and modulus of the open cylinder allows an effective *solid* cylinder (Figure 2.4 (b)) modulus to be defined through a simple scaling relation. The effective modulus of the solid cylinder will be less than that of the shell model, but the area-modulus product will be identical, i.e. (adapted from Thostenson and Chou [1]):

$$E_{solid} = \frac{A_{open}}{A_{solid}} \times E_{open} \tag{2.2}$$

This process yields Figure 2.5, where it can be seen that, depending on SWNT diameter, Young's modulus can vary drastically.

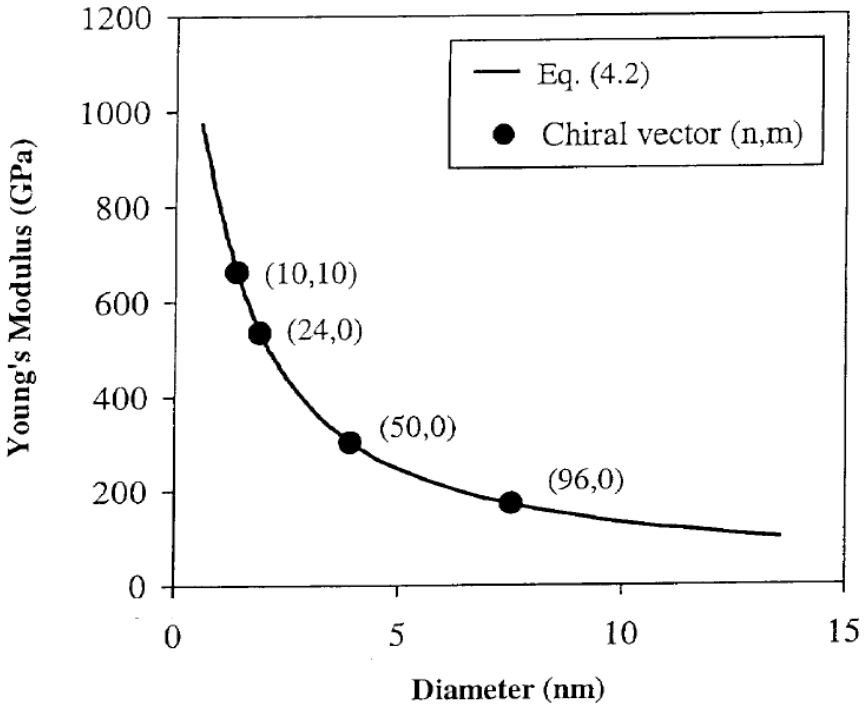

FIGURE 2.5. Young's modulus of SWNT vs diameter. [3]

A similar process and results are obtained for nanotube arrays, and one could extend the SWNT results to MWNTs by considering the added shell thickness from additional nanotubes.

With nearly all micromechanical models, the volume fraction of the reinforcement in the composite is used. However, as will be seen later, a majority of experimental work done with CNTs provide loadings in terms of weight. This necessitates a definition of a density to allow conversion from weight to volume. The same arguments and complications for defining a Young's Modulus apply to defining a density. Pipes et al. also tackle this discrepancy through a process similar to that described above except instead of assigning a modulus to the open cylinder, a mass is assigned, namely the mass of the carbon atoms comprising the shell. That mass is

then assumed to occupy the volume of the solid cylinder, giving an effective density. Figure 2.6 shows the result of this exercise.

Figures 2.5 and 2.6 clearly indicate the sensitivity of nanotube properties to its geometry, thus any attempt to predict CNT reinforcing capabilities in two or three-phase composites must begin with consideration of nanotube geometry.

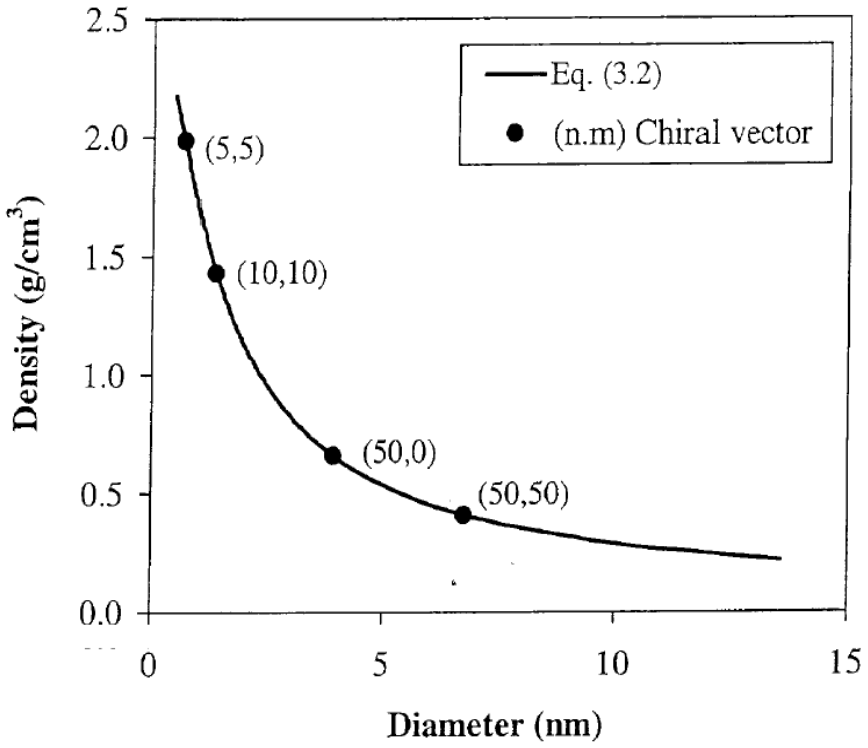

FIGURE 2.6. Density of SWNT vs diameter. [3]

2.2 Carbon Nanotube Reinforced Composites

Carbon nanotubes posses mechanical, thermal, and electrical properties which are equal or superior to any current materials which makes them an attractive candidate for enhancing a variety of matrices. They would offer immediate benefits in structures which cannot accommodate conventional reinforcement, such as polymer

fibers, foams, and films [10]. Their added benefit extends to conventional carbon fiber reinforced polymer composites (CFRPs) as well. CFRPs generally suffer from poor properties in off-fiber directions where material characteristics are dominated by matrix properties [11].

There exists two primary methods of incorporating CNTs in a conventional CFRP, either by grafting CNTs directly on to the microfiber surface, or by dispersing CNFs in the matrix material prior to manufacture. Both of these are depicted in Figure 2.7. Grafting CNTs on to microfibers is a relatively newer area of CNT reinforcement, and is not amenable to traditional micromechanical approaches nor an established manufacturing process. The process of grafting CNTs involves temperatures in the range of 700 to 1200 $^{\circ}C$, high enough to damage fiber mechanical properties [12]. The most tractable and economically feasible route of CNT incorporation is, at this point, adding CNTs directly to the matrix [11]. After CNTs are incorporated into the matrix, traditional manufacturing methods may be used to make two or three-phase composites (e.g. injection molding [13], prepregs with autoclave cure [14], VARTM [15]). For these reasons, the work presented here will focus on the case of adding CNTs directly to the matrix.

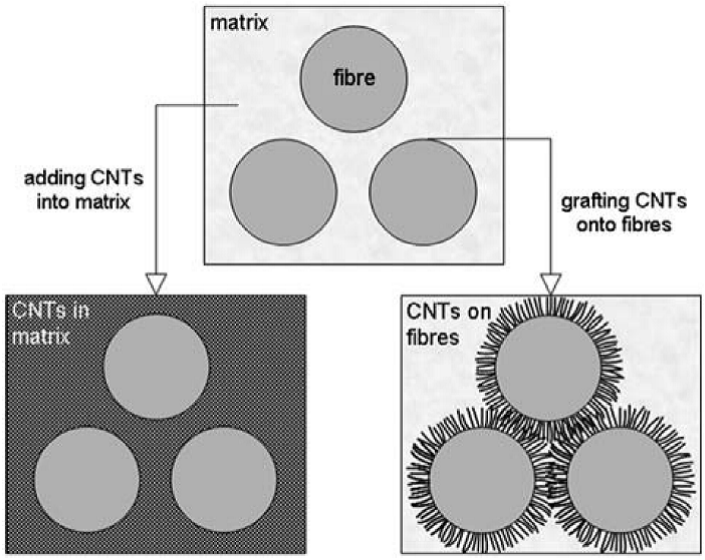

FIGURE 2.7. The two primary types of three-phase composites. [10]

There are four topics which any micromechanical model must address when predicting reinforcement capability of CNTs [16, 17, 18].

1. *Dispersion/Agglomeration of CNTs.* Nanotubes and other nanoreinforcements exhibit exceptionally high surface area to volume ratios compared to conventional reinforcements (see Figure 2.8). While beneficial to interfacial stress transfer, this large surface area also causes CNTs to have a strong tendency to bundle together to form agglomerations, which can act as defects in a two or three-phase composite [19]. Usually in micromechanical analyses, the assumption of uniform dispersion is made.

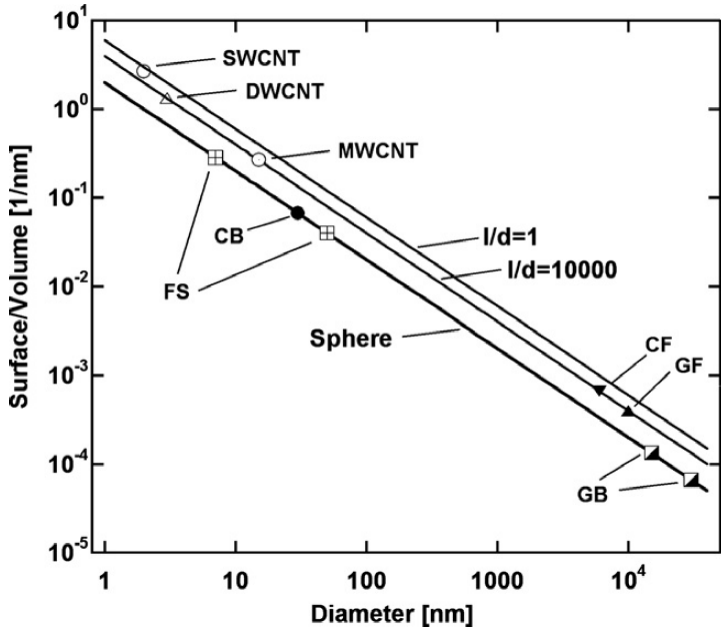

FIGURE 2.8. Surface area/volume vs diameter. [19]

2. *Orientation.* CNTs have been shown to be highly anisotropic, with off axis properties being an order of magnitude less than on axis [20, 21]. If nanotubes tend to orient in one direction more than others (as was done in Thostenson and Chou[1] and Mora et al. [22] through a drawing process), their anisotropy may be transferred to the composite.

3. *Length and Aspect Ratio.* Microfiber length has been known to be an important parameter for conventional composites for decades. Coleman et al. [18] present both a modified rule-of-mixtures and the Halpin-Tsai micromechanical models which incorporate length efficiency parameters. The general rule is that, the longer the fiber is, the more efficient it is due to an increased area available for stress transfer from the matrix to the fiber. This is expected to apply to nanotube reinforcements as well.

4. *Waviness.* Relatively little work has been done to model the effects tube waviness has on mechanical properties of CNT reinforced composites [16, 23, 24, 25]. It is common to see micromechanical approaches that consider CNTs straight to

simplify analyses [1, 13, 17, 26, 27, 28]. This simplification, however, usually leads to an overestimation of predicted stiffness due in large part to the fact that nanotubes are decidedly not straight in experimental settings (without special processes to encourage alignment, e.g. drawing). Figure 2.9 is a TEM image of MWNTs dispersed in a polystyrene matrix where one can see the varying degrees of curvature. This waviness degrades the reinforcing capabilities of CNTs and thus must be accounted for.

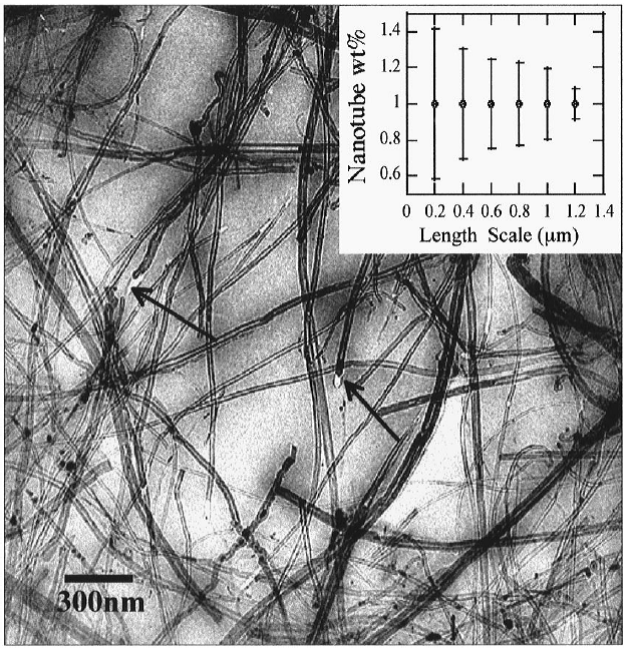

FIGURE 2.9. TEM image of a MWNT/polystyrene film. [29]

Interfacial shear strength between the fiber (whether CNF or microfiber) and matrix is an important parameter in the normal use of composites, but less so when making stiffness predictions. The perfect bonding assumption is made, and for low strain conditions, this assumption is valid.

2.3 Prediction of CNT Reinforced Composite Properties

Here, a review of micromechanical approaches published in literature is given. Sections are broken up for each different model used, with special attention being given as to how each addresses the four key points from section 2.2.

2.3.1 Rule-of-Mixture

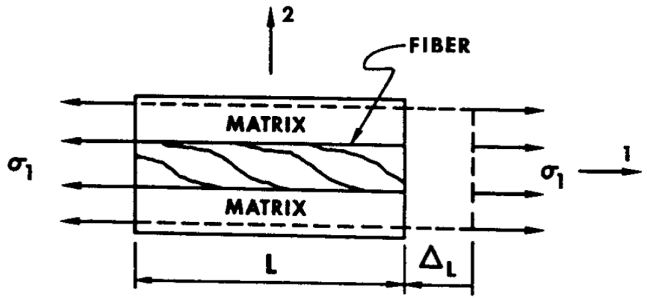

FIGURE 2.10. RVE for determination of tensile modulus. [30]

The Rule-of-Mixture is a mechanics of material approach which seeks to determine composite properties from the independent properties of the matrix and fiber and the volume fraction of the fiber. It yields simple algebraic relations for composite properties and, for on-axis properties (i.e. E_1 and ν_{12} referring to Figure 2.10), gives good results. If one assumes equal strain between fiber and matrix when subject to a strain σ_1, then the tensile modulus can be derived as (Jones [30]):

$$E_c = E_f v_f + E_m(1 - v_f) \tag{2.3}$$

Similar derivations can be made for the four other elastic properties (assuming a transversely isotropic lamina) and will not be repeated here.

Liu and Chen [27, 31] compared the rule of mixtures approach for short and long nanofibers with finite element predictions for a cylindrical representative volume element (RVE), shown in Figure 2.11.

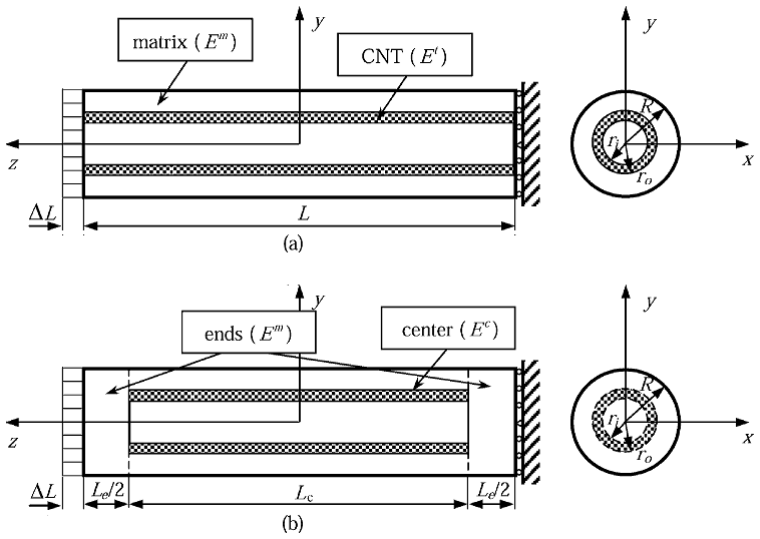

FIGURE 2.11. Cylindrical RVEs for long and short nanofibers. [31]

For the long CNT, the authors reported no difference between the rule-of-mixtures result for E_1 and finite element predictions. In the case of the short CNT, the RVE was subdivided in to three regions as shown, and tensile modulus was predicted using an *inverse* or *modified* rule-of-mixture in the form of (using notation from Figure 2.11):

$$\frac{1}{E_z} = \frac{1}{E_m}\left(\frac{L_e}{L}\right) + \frac{1}{E_c}\left(\frac{L_c}{L}\right)\left(\frac{A}{A_c}\right) \tag{2.4}$$

This method yielded modulus values only a few percent different from that of the finite element results. The long nanotube improved matrix modulus over 30% while the short nanotube improved reinforcement on the order of 5%. These studies demonstrated the potential for nanotube reinforcement and how that potential is

influenced by length. They did not address the characteristic waviness and varying orientation nanotubes can take when infused with a matrix.

Griebel and Hamaekers [17] and Frankland et al. [32] conducted molecular dynamics (MD) simulations on two RVEs very similar to that of Liu and Chen [27, 31], Figure 2.11. Rule of mixtures and molecular dynamics predictions for long nanofiber are shown in Figure 2.12. It can be seen that the rule of mixtures agrees well with MD results, especially at low strains ($< 2\%$). Again, however, these models do not address waviness or orientation.

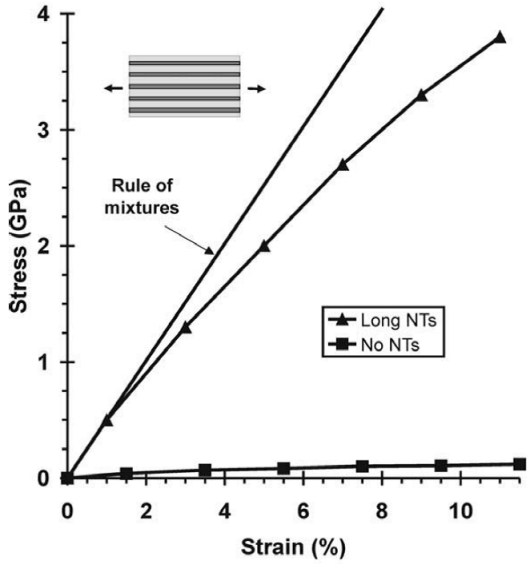

FIGURE 2.12. Stress-strain curve from molecular dynamics simulations. [32]

Coleman et al. [18] presents the rule of mixtures with two added terms to account for orientation and length effects in the form of:

$$E_c = (\eta_o \eta_l E_f - E_m) V_f + E_m \tag{2.5}$$

where η_o accounts for orientation effects and η_l for length effects. For aligned fibers, fibers oriented in plane, and random orientation of fiber, η_o takes the values of 1, 3/8, 1/5 respectively. η_l is a function of fiber length, diameter, tensile modulus, volume fraction, and the modulus of the matrix.

Omidi et al. [33] is the only rule of mixtures model reviewed which incorporates length, orientation, and waviness of nanotubes. This model uses the same length and orientation parameters as Coleman et al. [18], but adds two additional terms (presented in modified form for comparison with other rules of mixture):

$$E_c = (\eta_o \eta_l \eta_\omega E_f - E_m) V_f e^{\alpha V_n t} + E_m \tag{2.6}$$

where $\eta_\omega = 1 - \frac{a}{w}$ and a and w are the amplitude and wavelength of an assumed sinusoidally-wavy nanotube. The exponential term is used to account for the non-linear relationship between nanotube volume fraction and Young's Modulus at higher loadings. The authors report good agreement with experimental results, as evidenced by Figure 2.13 [33]. However, judging by the results of other micromechanical models to be presented, the linear degredation of CNT modulus with increasing waviness ($\frac{a}{w}$) is not sufficient to capture how rapidly the modulus is reduced. Many studies [16, 21, 23, 24, 25] report highly non-linear reduction of modulus. For example, for a nanotube to matrix modulus ratio of 1000 (a typical value), increasing waviness from 0 (perfectly straight) to 0.1 results in a 50% loss of composite stiffness.

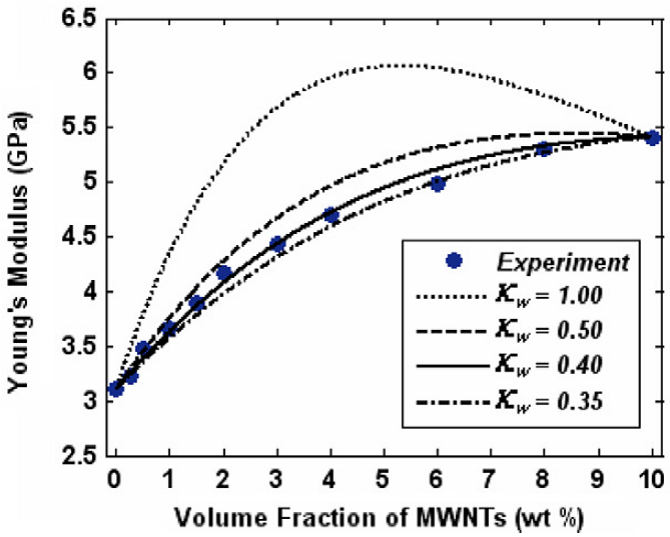

FIGURE 2.13. Modulus vs MWNT volume fraction for various waviness values. [33]

2.3.2 Halpin-Tsai

The Halpin-Tsai equations are a set of semi-empirical relationships which are "handy forms" of Hill's generalized self-consistent micromechanical model [34]. They have gained wide spread use for composite material predictions due to their simultaneous simplicity and accuracy. The equations exist in several forms, depending on reinforcement packing and orientation. For a composite reinforced with randomly oriented fibers and including length effects, the Halpin-Tsai equations take the form [18]:

$$\frac{E_c}{E_m} = \frac{3}{8}\left[\frac{1+\eta_l v_f}{1-\eta_l v_f}\right] + \frac{5}{8}\left[\frac{1+2\eta_t v_f}{1-\eta_t v_f}\right] \tag{2.7}$$

where:

$$\eta_l = \frac{E_f/E_m - 1}{E_f/E_m + 2(l/d)_f} \qquad \text{and} \qquad \eta_t = \frac{E_f/E_m - 1}{E_f/E_m + 2} \tag{2.8}$$

Figure 2.14 shows experimental results of Kanagaraj et al. [13] plotted against Equation 2.7 predictions. Despite the apparent good agreement with experimental

results, waviness was not considered in this study. Two possibilities for this good agreement despite disregarding waviness are:

1. The authors reported aspect ratios in the range of 50-250, though no distribution is identified. If the nanotubes were predominantly lower in aspect ratio, the assumption of zero waviness would be closer to reality since shorter tubes are more resistant to bending.

2. A MWNT modulus of $910GPa$ is used. Depending on the thickness of the MWNT, this may or may not be a good estimation. If modulus used in predictions is too high, it may make up for the actual reduced modulus in experiment.

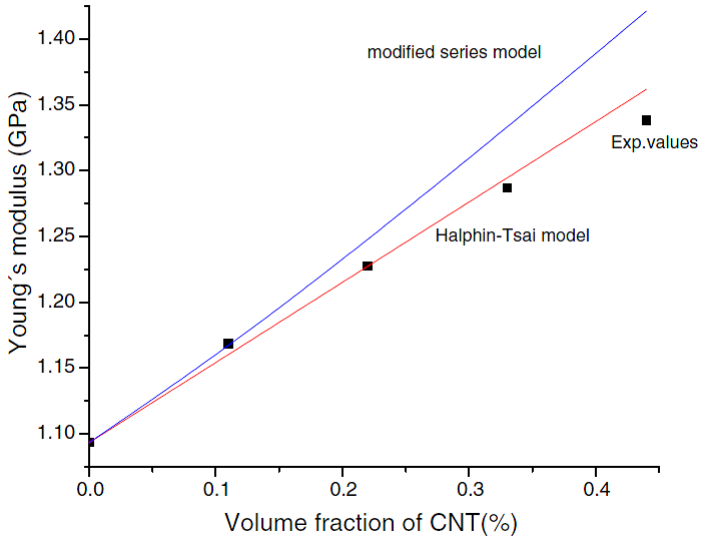

FIGURE 2.14. Halpin-Tsai predictions for CNT reinforced high-density polyethylene. [13]

2.3.3 Mori-Tanaka

The Mori-Tanaka method is another micromechanical construct but with the additional ability to model interactions between inclusions (in this case, nanotubes).

The details of this method are beyond the scope of this work, but for completeness it is noted that several authors report good results using this method. Fisher et al. [16] and Odegard et al. [26] used the Mori-Tanaka model to predict reinforcement of straight, randomly distributed, and randomly oriented nanotubes. Seidel et al. [28] and Shi et al. [21] used it to address agglomeration of CNTs, with the former considering straight fibers and the latter considering wavy fibers. Yanase et al. [25] employed the model including waviness effects through Hsaio and Daniel's [35] model for wavy microfibers.

2.3.4 Anumandla-Gibson Model

Anumandla and Gibson [23] presented a comprehensive micromechanics model which has several attractive features. It is based on existing micromechanics models, and produces simple algebraic equations to predict CNT reinforced composite properties. The model captures key expected behaviors, such as drastic modulus reduction with increasing waviness and random fiber orientation, and compares well with experimental results. Chapter 3 reproduces the model in detail and discusses its strengths and weaknesses. Chapter 4 then compares predictions with experimental results from literature.

CHAPTER 3

METHODS

3.1 Anumandla-Gibson

3.1.1 Mathematical Development

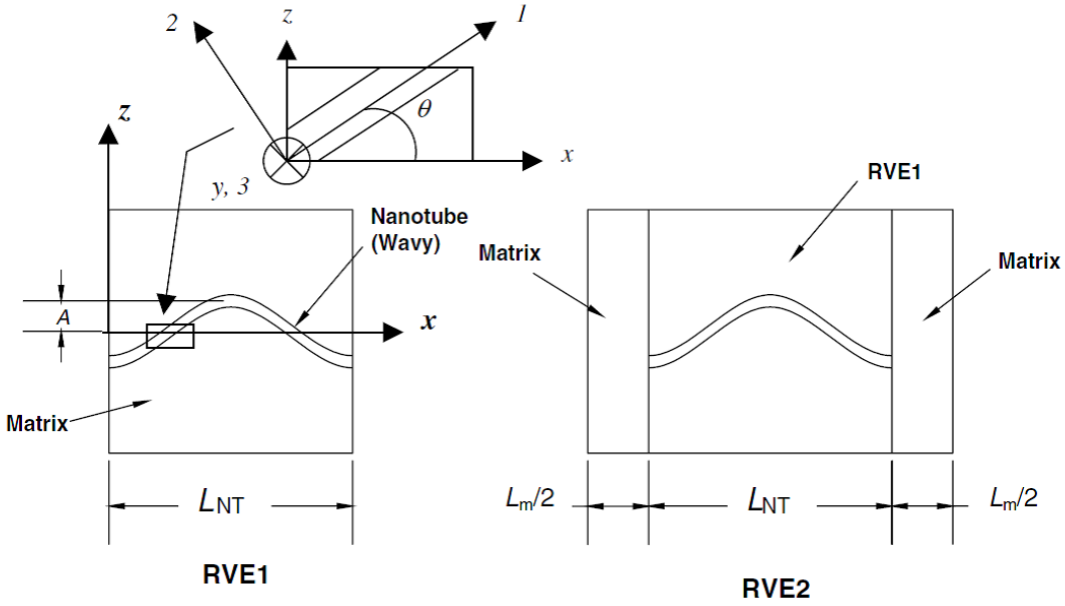

FIGURE 3.1. RVEs used in A-G model. [23]

The Anumandla-Gibson model uses a two-RVE approach, as depicted in Figure 3.1. The first step in the process is to estimate the properties of RVE1. At this point it is assumed that the fiber is straight, isotropic, and since it spans the entire RVE, is continuous. The Chamis [36] micromechanics equations are used for

this and take the form:

$$E_{11} = v_f E_f + v_m E_m \tag{3.1}$$

$$E_{22} = E_{33} = \frac{E_m}{1 - \sqrt{v_f}\left(1 - \frac{E_m}{E_f}\right)} \tag{3.2}$$

$$G_{12} = G_{13} = G_{23} = \frac{G_m}{1 - \sqrt{v_f}\left(1 - \frac{G_m}{G_f}\right)} \tag{3.3}$$

$$\nu_{12} = \nu_{13} = v_f \nu_f + v_m \nu_m \tag{3.4}$$

$$\nu_{23} = \frac{E_{22}}{2G_{12}} - 1 \tag{3.5}$$

With the properties of RVE1 now known, RVE1 compliances (for a zero-fiber-waviness condition) can be calculated. Assuming a thin unidirectional lamina under plane stress, the compliances are (Daniel and Ishai [37]):

$$S_{11} = 1/E_{11} \tag{3.6}$$

$$S_{22} = 1/E_{22} \tag{3.7}$$

$$S_{12} = S_{21} = -\frac{\nu_{12}}{E_{11}} = -\frac{\nu_{21}}{E_{22}} \tag{3.8}$$

$$S_{66} = \frac{1}{G_{12}} \tag{3.9}$$

Effects of fiber waviness may now be included. Hsaio and Daniel [35] take an RVE similar to that of RVE1 in Figure 3.1 and slice it in to infinitesimal pieces of width dx. Each slice is treated as an off-axis lamina whose properties may be calculated using standard micromechanical approaches and transformed using the standard transformation matrix. Averaging the strains over one wavelength of waviness and having knowledge of the applied stresses allows calculation of *effective*

properties of the form (Hsiao and Daniel [35]):

$$E_x = \frac{\sigma_x}{\bar{\epsilon_x}} = \frac{1}{S_{11}I_1 + (2S_{12} + S_{66})\, I_3 + S_{22}I_5} \tag{3.10}$$

$$\nu_{xz} = \frac{\bar{\epsilon_z}}{\epsilon_x} = \frac{[(S_{11} + S_{22} - S_{66})\, I_3 + S_{12}\,(I_1 + I_5)]}{S_{11}I_1 + (2S_{12} + S_{66})\, I_3 + S_{22}I_5} \tag{3.11}$$

$$G_{yz} = \frac{1}{2\,(S_{22} - S_{23})\, I_6 + S_{66}I_8} \tag{3.12}$$

$$G_{xz} = \frac{1}{4\,(S_{11} + S_{22} - 2S_{12})\, I_3 + S_{66}\,(I_1 - 2I_3 + I_5)} \tag{3.13}$$

The I terms account for of waviness, and are defined as:

$$I_1 = \frac{1 + \alpha^2/2}{(1+\alpha^2)^{\frac{3}{2}}} \quad I_3 = \frac{\alpha^2/2}{(1+\alpha^2)^{\frac{3}{2}}} \quad I_5 = 1 - \frac{1 + 3\alpha^2/2}{(1+\alpha^2)^{\frac{3}{2}}} \quad I_6 = \frac{1}{(1+\alpha^2)^{\frac{1}{2}}} \quad I_8 = 1 - I_6 \tag{3.14}$$

where $\alpha = 2\pi\left(\frac{A}{L_{NT}}\right)$ and A/L_{NT} is the degree of waviness, quantified by the ratio of the amplitude of the sinusoid to the length of RVE1. This ratio will henceforth be referred to as the "wavy factor." Wavy factors of 0, 5, 10, 25, and 50% are used in modulus vs volume fraction plots to be shown.

The transverse plane strain bulk modulus must be calculated, which requires bulk moduli for the fiber and matrix. These are as follows:

$$K_f = \frac{E_f}{2(1 - 2\nu_f)(1 + \nu_f)} \tag{3.15}$$

$$K_m = \frac{E_m}{2(1 - 2\nu_m)(1 + \nu_m)} \tag{3.16}$$

$$K_{zy} = K_2 = \frac{(K_f + G_m)K_m + (K_f - K_m)G_m v_f}{(K_f + G_m) - (K_f - K_m)v_f} \tag{3.17}$$

Orientation effects are then incorporated through the model of Christensen and Waals [38], with RVE1 strains being averaged over all possible orientations of the nanotube.

This gives an effective isotropic modulus and Poisson ratio for RVE1 in the form of:

$$\tilde{E} = E_{3D-RVE1} = \frac{[E_x + (4\nu_{xz}^2 + 8\nu_{xz} + 4)K_{zy}][E_x + (4\nu_{xz}^2 - 4\nu_{xz} + 1)K_{zy} + 6(G_{zy} + G_{zy})]}{3\,[2E_x + (8\nu_{xz}^2 + 12\nu_{xz} + 7)K_{zy} + 2(G_{xz} + G_{zy})]} \tag{3.18}$$

$$\tilde{\nu} = \nu_{3D-RVE1} = \frac{E_x + (4\nu_{xz}^2 + 16\nu_{xz} + 6)K_{zy} - 4(G_{xz} + G_{zy})}{4E_x + (16\nu_{xz}^2 + 24\nu_{xz} + 14)K_{zy} + 4(G_{xz} + G_{zy})} \tag{3.19}$$

It is important to note here that Christensen and Waals assume transverse isotropy. For a straight nanofiber (0% wavy factor), this assumption is applicable. However, as the wavy factor is increased, portions of the embedded nanotube of RVE1 begin to align along the transverse (z in Figure 3.1) direction. This would violate the transversely isotropic assumption, making RVE1 generally orthotropic. Despite this, the model keeps the transverse isotropy assumption. Waviness induced degradation of tensile modulus is captured in E_x, but increased transverse stiffness is not accounted for.

An effective isotropic modulus and Poisson ratio for RVE2 is then computed using an inverse rule of mixtures, similar to that of Equation 2.4.

$$\frac{1}{E_{3D-RVE2}} = \frac{1}{E_{3D-RVE1}}\left(\frac{L_{NT}}{L_m + L_{NT}}\right) + \frac{1}{E_m}\left(\frac{L_m}{L_m + L_{NT}}\right) \tag{3.20}$$

$$\frac{1}{\nu_{3D-RVE2}} = \frac{1}{\nu_{3D-RVE1}}\left(\frac{L_{NT}}{L_m + L_{NT}}\right) + \frac{1}{\nu_m}\left(\frac{L_m}{L_m + L_{NT}}\right) \tag{3.21}$$

3.1.2 Sensitivities

3.1.2.1 Volume fraction inside RVE1.

In conventional micromechanical analyses of microfiber composites, RVEs similar to Figure 3.1 are used, with the exception that the area of RVE1 is entirely composed of fiber material. To define a volume fraction of RVE1 for microfiber analysis would be nonsense since, by definition, the

fiber volume fraction would always be 100%. Thus, the volume fraction of the composite would be completely defined by the length ratios of the segments in the RVE, L_{NT} and L_m here. This is not the case with the A-G model.

The Chamis equations that are employed to calculate RVE1 mechanical properties in subsection 3.1.1 contain the fiber volume fraction term v_f. This volume fraction is not, however, the fiber volume fraction for the composite since RVE2 has added the two sections of matrix material on either end of RVE1. The volume fraction in RVE1 must therefore be greater than the composite volume fraction (i.e. RVE2 volume fraction). The volume fraction inside of RVE1, ν_{f-RVE1}, must satisfy the relationship

$$v_{f-composite} = v_{f-RVE1}\left(\frac{L_{NT}}{L_m + L_{NT}}\right) \tag{3.22}$$

to ensure composite volume fraction reflects reality. This equation contains two related unknowns, which leaves two possible routes of solving it. One must either choose a value for the ratio of L_{NT}/L_m and solve for RVE1 volume fraction, or select a value for ν_{f-RVE1} and solve for the length ratio. Since neither of these are physical properties of the nanotube or matrix, it is difficult to get an idea of what value they should take.

To add to this, predictions made by the A-G model are particularly sensitive to the choice of RVE1 volume fraction. If we define v_{f-RVE1} as:

$$v_{f-RVE1} = v_{f-composite} + v_{f-added} \tag{3.23}$$

where $\nu_{f-added}$ is an arbitrary additional volume fraction percentage over the composite's volume fraction, it is possible to test the sensitivity of the model to $\nu_{f-added}$. Figures 3.2 and 3.3 depict results using $\nu_{f-added}$ values of 1 and 10% for a 1% CNF volume fraction composite. These graphs show the vastly different modulus predicted for each case. For example, at 25% volume loading and zero waviness, the

$\nu_{f-added} = 1\%$ case predicts a modulus of about $17GPa$ whereas the $\nu_{f-added} = 10\%$ predicts about $3.4GPa$. In chapter 4 a $\nu_{f-added}$ of 5% is used since it provides reasonable predictions compared to experimental results and other models, as will be seen.

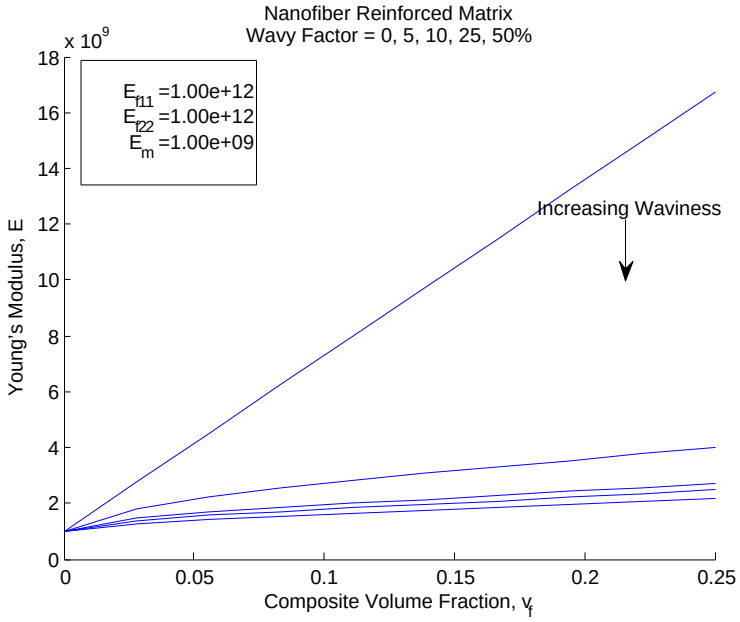

FIGURE 3.2. 1% additional CNF volume fraction in RVE1 ($v_{f-added} = 1\%$).

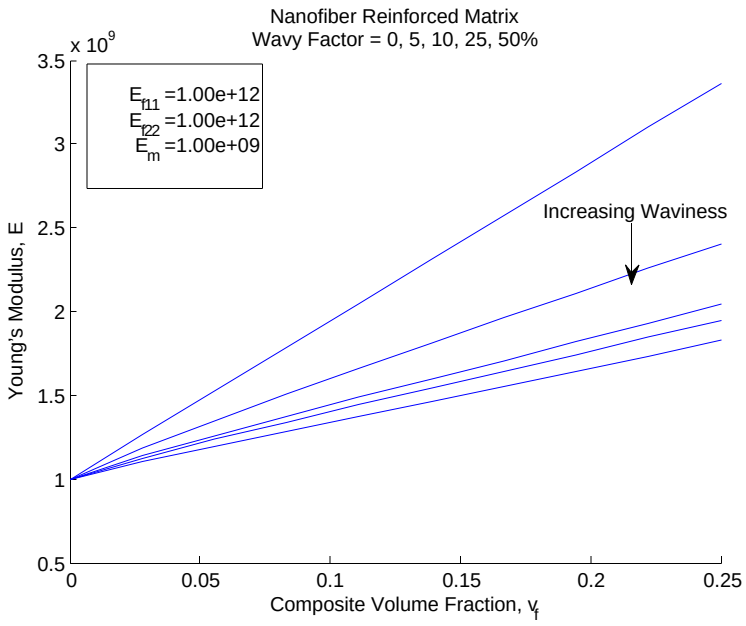

FIGURE 3.3. 10% additional CNF volume fraction in RVE1 ($v_{f-added} = 10\%$).

3.1.2.2 Micromechanical model in RVE1. In the Anumandla-Gibson model, there are actually two sets of micromechanical equations that are used. The Chamis equations are used to predict RVE1 properties, and an inverse rule of mixtures is used to predict RVE2 properties. It is not immediately clear how appropriate the Chamis equations are for use here, so they were replaced by the Halpin-Tsai equations to gauge if either had an advantage over the other. The Halpin-Tsai equations, for microfiber composites, are known to fit experimental data well at low volume fractions [18]. Since CNT composites are almost exclusively fabricated at low loadings ($\leq 10\%$), the Halpin-Tsai model may show improvement over the Chamis model.

The generalized Halpin-Tsai model is as follows [39]:

$$\frac{\bar{P}_c}{P_m} = \frac{1 + \zeta\eta v_f}{1 - \eta v_f} \tag{3.24}$$

where

$$\eta = \frac{\frac{P_f}{P_m} - 1}{\frac{P_f}{P_m} + \zeta} \tag{3.25}$$

$\bar{P}_c$ is a composite property (E_{22}, G_{12}, or ν_{23}), and P_m or P_f is the corresponding matrix or fiber property. ζ is a measure of reinforcement and depends on boundary conditions. Generally accepted values used for ζ are:

TABLE 3.1. Halpin-Tsai Parameter Values

Property	ζ	Reference
E_{22}	2	[39]
G_{12}	$1 + 40v_f^{10}$	[30]
ν_{23}	1	

For E_{11} and ν_{12}, ζ takes on a very large value for continuous fiber composites. In the limit as $\zeta \to \infty$, the Halpin-Tsai equations reduce to the rule of mixture. Thus the rule of mixture (Equation 2.3) is used in calculation of these properties. It should be noted that Equation 3.24 and Equation 2.7 are equivalent, with the exception that Equation 3.24 is a more generalized form, applicable to short and long fiber composites, depending on choice of parameters.

Figure 3.4 shows the result of this exercise. It can be seen for zero waviness, the two models produce identical results, which is expected. However, with increasing waviness, the Halpin-Tsai model shows a quicker reduction in modulus. At sufficiently low loadings and high waviness, the Halpin-Tsai equations actually predict a *reduction* in modulus. Chapter 4 will compare both the Chamis and Halpin-Tsai predictions to experimental results.

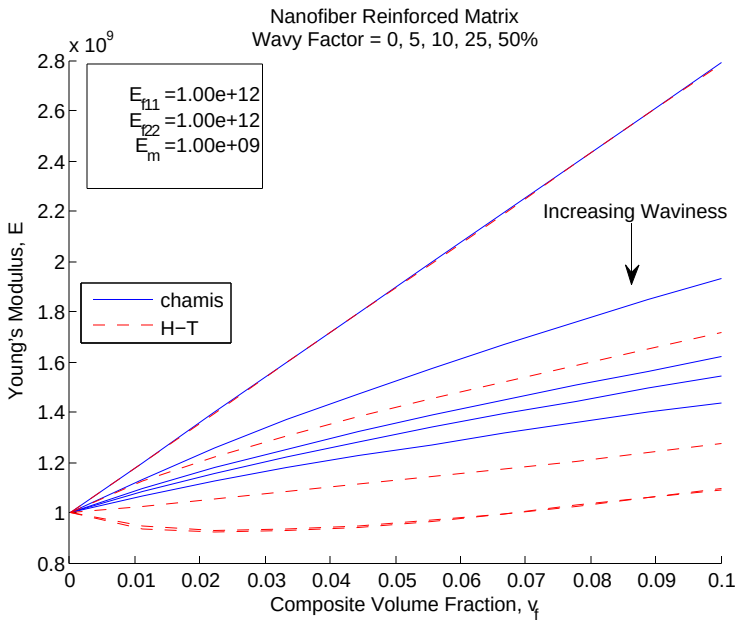

FIGURE 3.4. Results for Chamis and Halpin-Tsai models used in RVE1.

3.1.2.3 Isotropic vs transversely isotropic CNFs. One of the key simplifying assumptions made in the A-G model is that the embedded nanotube is isotropic. Though, as was previously mentioned in section 2.2, nanotubes are decidedly *not* isotropic. It is desired to see how large of an impact this assumption has on model predictions.

The Chamis and Halpin-Tsai micromechanical models are able to handle transversely isotropic reinforcement, so no modification of the equations are necessary. What is needed are representative off-axis nanotube properties. Several research efforts have been made to predict these properties, and Table 3.2 gives values selected for simulation.

Figures 3.5 and 3.6 depict predictions using an isotropic and a transversely isotropic fiber. The difference between the plots is negligible. For example, at 5% waviness and 25% volume fraction each model predicts values shown in Table 3.3.

TABLE 3.2. Transversely Isotropic CNT Properties

Property	Value	Reference
E_{11}	$1TPa$	[4] ((9,0) High AR uncapped)
E_{22}	$68.3GPa$	[20]
G_{12}	$0.37TPa$	[40] (1 CNT wall torsion test)
ν_{12}	0.3	[23]
ν_{23}	0.34	[20]

TABLE 3.3. RVE2 Sample Results for Isotropic and Transversely Isotropic CNFs, 5% waviness, 25% Volume Fraction

Model	Case	
	Isotropic	Transversly Isotropic
Chamis	$2.987GPa$	$2.981GPa$
Halpin-Tsai	$2.643GPa$	$2.629GPa$

Similar results are seen for other volume fractions and waviness values. These suggest that considering a fiber to be isotropic is a good assumption for this model. This is likely due to nanofibers being assumed to be uniformly dispersed and randomly oriented, along with the fact that primary stiffness contributions come from the nanotubes' exceedingly high tensile modulus.

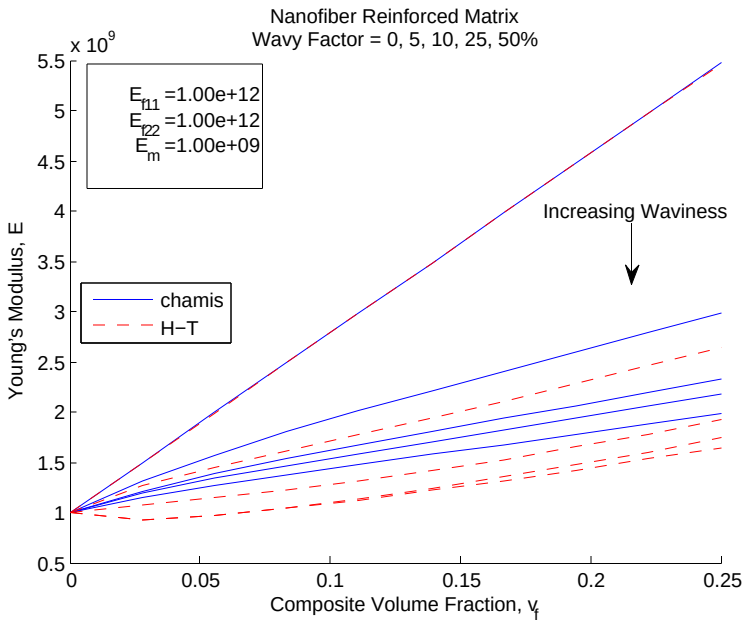

FIGURE 3.5. Waviness plot for isotropic fiber.

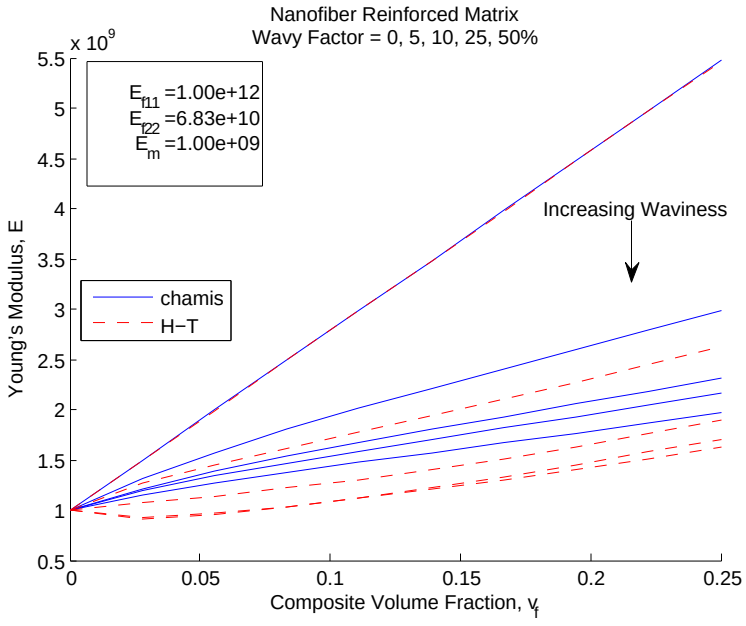

FIGURE 3.6. Waviness plot for transversely isotropic fiber.

3.1.2.4 Nanotube form. As mentioned in chapter 2, nanotubes come in various forms. This (and other) micromechanical model makes no distinction between, for example, a single-walled or multi-walled nanotube, and considers all to be solid. For stiffness predictions, this assumption seems to be a good one since experimental and model results show fair agreement in chapter 4. This would probably not be the case if composite strength was under consideration. For example, SWNTs and MWNTs have different failure modes, where MWNTs have a tendency to undergo a "sword in sheath" failure where nanotube layers slide relative to each other [18]. This isn't possible in a SWNT since it is only one layer.

3.2 Classical Laminated Plate Theory

Details of classical laminated plate theory relevant to this work are adapted from [37] and presented here. In-depth explanations are available in several composites analysis books and reports[30, 35, 41, 42].

There are eight basic assumptions CLPT makes [37, 41]:

1. Each layer of the laminate is quasi-homogenous and orthotropic
2. The laminate thickness is very small compared to its other dimensions
3. All displacements are small compared with the thickness of the laminate
4. Displacements are continuous throughout the laminate
5. In-plane displacements vary linearly through the thickness of the laminate.
6. Straight lines normal to the middle surface remain straight and normal to that surface after deformation.
7. Strain-displacement and stress-strain relations are linear
8. Normal distances from the middle surface remain constant.

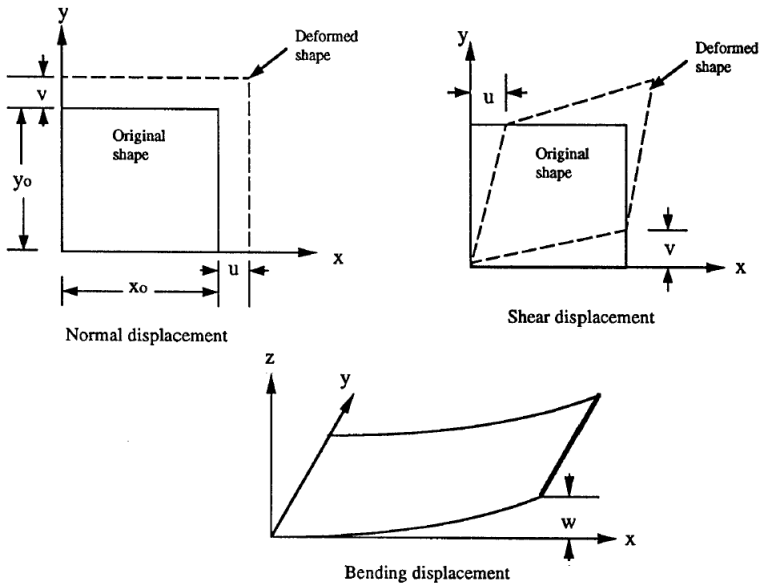

Figure 4. Displacements of a plate.

FIGURE 3.7. Strain definitions for CLPT. [41]

The stress-strain relations for each individual lamina, in its own coordinate system is (1-direction along the fiber):

$$\begin{bmatrix} \sigma_1 \\ \sigma_2 \\ \tau_6 \end{bmatrix} = \begin{bmatrix} Q_{11} & Q_{12} & 0 \\ Q_{21} & Q_{22} & 0 \\ 0 & 0 & Q_{66} \end{bmatrix} \begin{bmatrix} \epsilon_1 \\ \epsilon_2 \\ \gamma_6 \end{bmatrix} \tag{3.26}$$

Where the Q (stiffness) terms are defined as follows:

$$Q_{11} = \frac{E_1}{1 - \nu_{12}\nu_{21}} \tag{3.27}$$

$$Q_{22} = \frac{E_2}{1 - \nu_{12}\nu_{21}} \tag{3.28}$$

$$Q_{12} = Q_{21} = \frac{\nu_{21}E_1}{1 - \nu_{12}\nu_{21}} = \frac{\nu_{12}E_2}{1 - \nu_{12}\nu_{21}} \tag{3.29}$$

$$Q_{66} = G_{12} \tag{3.30}$$

The elastic moduli (E_1, E_2), shear modulus (G_{12}), and Poisson ratio (ν_{12}) are that of the laminate. These must be estimated by yet another micromechanical model. If a CNT reinforced matrix is used, it would be accounted for here.

To do this, the Halpin-Tsai model used in section 3.1.2.2 is also used here with the same parameters. This gives us knowledge of on-axis properties. If the lamina is off-axis in lay-up, then these properties must be transformed in to the global laminate system, x (0°) and y (90°). This is done as follows:

$$\begin{bmatrix} Q_{xx} & Q_{xy} & 2Q_{xs} \\ Q_{yx} & Q_{yy} & 2Q_{ys} \\ Q_{sx} & Q_{sy} & 2Q_{ss} \end{bmatrix} = [T^{-1}] \begin{bmatrix} Q_{11} & Q_{12} & 0 \\ Q_{21} & Q_{22} & 0 \\ 0 & 0 & 2Q_{66} \end{bmatrix} [T] \tag{3.31}$$

where T is the transformation matrix defined as:

$$[T] = \begin{bmatrix} \cos^2\theta & \sin^2\theta & 2\cos\theta\sin\theta \\ \sin^2\theta & \cos^2\theta & -2\cos\theta\sin\theta \\ -\cos\theta\sin\theta & \cos\theta\sin\theta & \cos^2\theta - \sin^2\theta \end{bmatrix} \tag{3.32}$$

and θ is the off-axis angle of the ply, depicted in Figure 3.8.

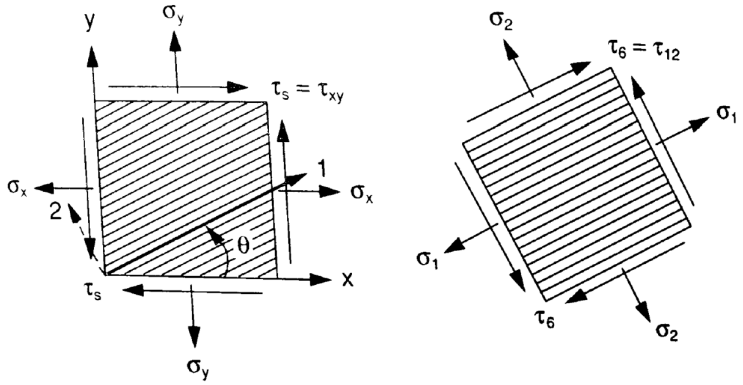

FIGURE 3.8. Off-axis lamina with stress transformation. [37]

Stresses may be related to strains at the laminate level now as:

$$[\sigma]^k_{x,y} = [Q]^k_{x,y}[\epsilon^0]_{x,y} + z[Q]^k_{x,y}[\kappa]_{x,y} \tag{3.33}$$

where ϵ^0 are the midplane (x-y plane in Figure 3.9) strains, z is the z coordinate of the k'th ply, and κ are the laminate curvatures. We can define forces per length and moments per length on the x-z and y-z planes as:

$$\begin{bmatrix} N_x \\ N_y \\ N_s \end{bmatrix} = \sum_{k=1}^{n} \int_{z_{k-1}}^{z_k} \begin{bmatrix} \sigma_x \\ \sigma_y \\ \tau_s \end{bmatrix}_k dz \quad \text{and} \quad \begin{bmatrix} M_x \\ M_y \\ M_s \end{bmatrix} = \sum_{k=1}^{n} \int_{z_{k-1}}^{z_k} \begin{bmatrix} \sigma_x \\ \sigma_y \\ \tau_s \end{bmatrix}_k z dz \tag{3.34}$$

Substituting Equation 3.33 in to Equation 3.34, carrying out the integral, and rearranging gives the relationship between laminate forces, moments, and strains in the form of:

$$\begin{bmatrix} N \\ M \end{bmatrix} = \begin{bmatrix} A & B \\ B & D \end{bmatrix} \begin{bmatrix} \epsilon^0 \\ \kappa \end{bmatrix} \tag{3.35}$$

where A, B, and D are the 3x3 laminate stiffness matrices, defined as:

$$A_{ij} = \sum_{k=1}^{n} Q^k_{ij}(z_k - z_{k-1}) \tag{3.36}$$

$$B_{ij} = \frac{1}{2} \sum_{k=1}^{n} Q^k_{ij}(z_k^2 - z_{k-1}^2) \tag{3.37}$$

$$D_{ij} = \frac{1}{3} \sum_{k=1}^{n} Q^k_{ij}(z_k^3 - z_{k-1}^3) \tag{3.38}$$

Inverting the laminate stiffness matrices gives laminate compliances.

$$\begin{bmatrix} a & b \\ c & d \end{bmatrix} = \begin{bmatrix} A & B \\ B & D \end{bmatrix}^{-1} \tag{3.39}$$

At this point, laminate properties can be extracted as follows, defining the laminate thickness as h,

$$\bar{E}_x = \frac{1}{ha_{xx}} \qquad \bar{E}_y = \frac{1}{ha_{yy}} \qquad \bar{G}_{xy} = \frac{1}{ha_{ss}} \qquad \bar{\nu}_{xy} = -\frac{a_{yx}}{a_{xx}} \qquad \bar{\nu}_{yx} = -\frac{a_{xy}}{a_{yy}} \quad (3.40)$$

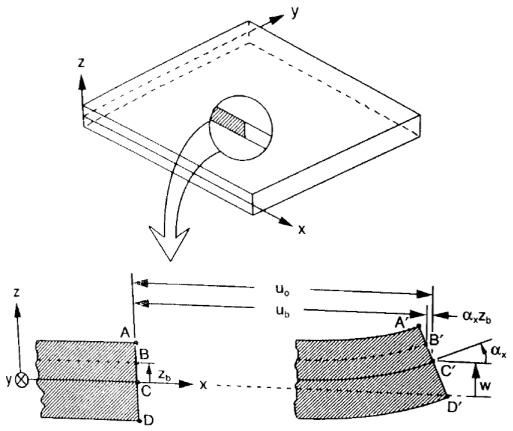

FIGURE 3.9. Laminate section before and after deformation. [37]

CHAPTER 4

RESULTS AND EXPERIMENTAL COMPARISON

4.1 Two-Phase Composites

In the original publication of the A-G model, Anumandla [23] compared model predictions to published experimental results from Andrews et al [43]. This comparison was recreated in Figure 4.1 to ensure MATLAB implementation matched results from the original publication, and to additionally compare results using the Halpin-Tsai modification from section 3.1.2.2.

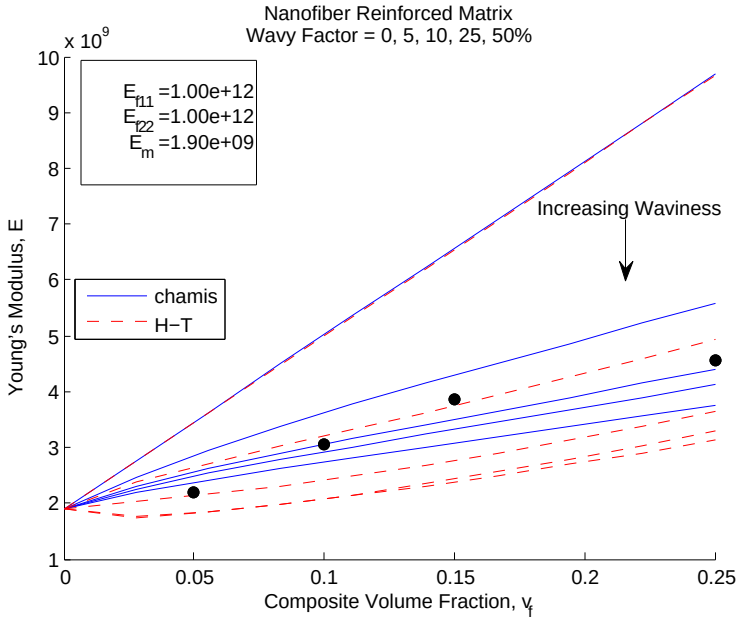

FIGURE 4.1. Andrews et al. experimental data. [43]

Good agreement is seen between experimental and theoretical results, but this is limited to one dataset. A literature survey was done to collect additional experimental results for comparison, the results of which are shown in figures 4.2 through 4.7. All plots show moduli of fiber and matrix. Numerical data and assumptions that went in to each plot can be found in the appendix.

On reviewing the plots generated comparing experimental and model results, several trends can be identified. For the Chamis implementation, a decent portion of experimental results lie between 5-25% waviness, which agrees well with Anumandla's [23] original conclusion. For the Halpin-Tsai model, nearly all experimental results lie between the 0 and 10% waviness lines, which gives a narrower band of waviness values than does the Chamis model. Having this small band of lower waviness values is important since, as discussed in subsection 3.1.1, higher wavy factors violate transverse isotropy more. To add to this, 0 to 10% waviness seems more realistic given the high aspect ratios typical of nanotubes. Some experimental results agree with the 25 and 50% wavy factor lines of the Chamis implementation. In reality, with nanotube lengths being on the order of millimeters, this could mean the wavy amplitude is several hundred diameters. This qualitatively does not agree with Figure 2.9 or other SEM/TEM nanocomposite images seen in literature.

Omidi et al. [33] had the most outlying data points. Below volume fractions of about 4%, experimental values followed the trend of the 0% waviness lines, but at slightly higher modulus values. Data for volume fractions between 4 and 10% fell in between the 0 and 5% waviness lines of each model. A possible explanation for this is the method of manufacture of the test specimen used in the study. Test coupons were fabricated through casting in this case. Depending on the flow in to the mold, there could have been some bias towards a particular direction in alignment of nanotubes. The authors also state that samples were mechanically polished prior to testing. Thostensen and Chou [1] prepared MWNT/Polystyrene samples using a

microtome cutting process and reported distortion of nanotubes in the cutting direction, meaning the cutting process influenced tube alignment. Details are not given on the mechanical polishing of Omidi et al. but if polishing was done along one direction it could again make the nanotubes tend along the cutting plane, which would violate the random alignment assumption.

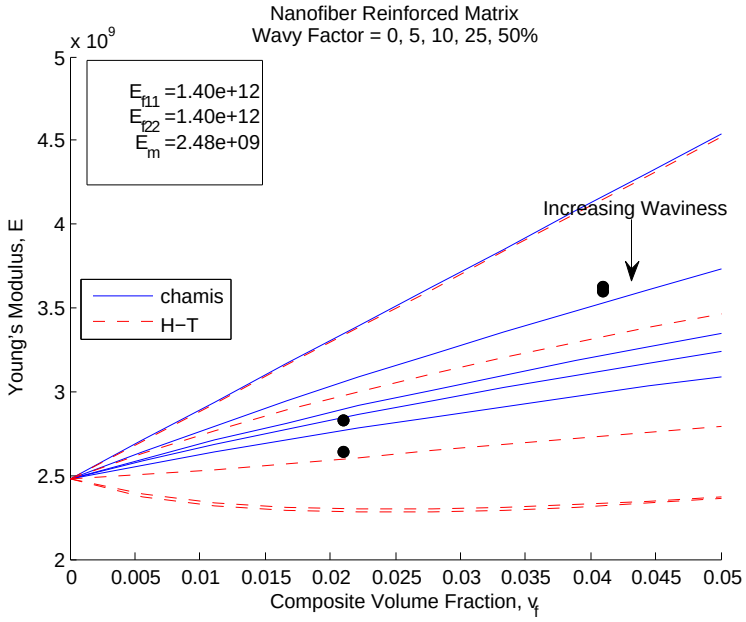

FIGURE 4.2. Iwahori et al. experimental data. [44]

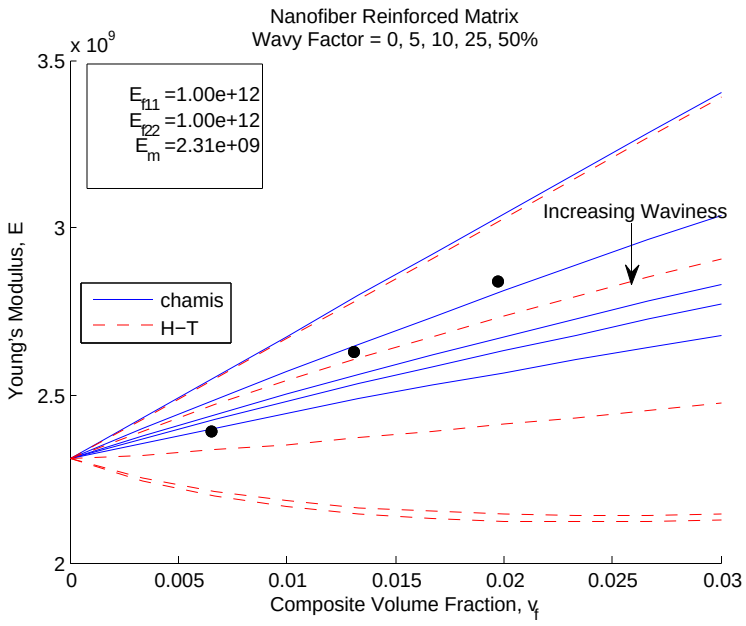

FIGURE 4.3. Zhou et al. experimental data (0.02/min strain rate). [15]

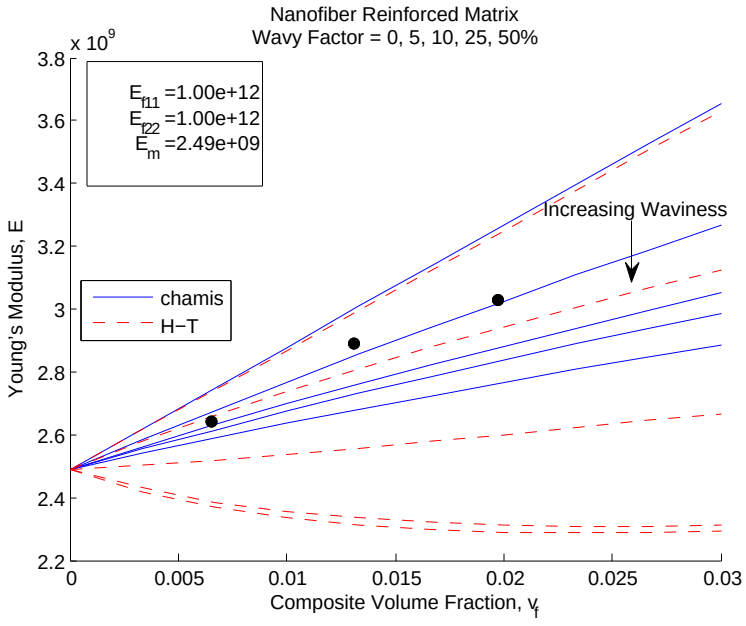

FIGURE 4.4. Zhou et al. experimental data (0.20/min strain rate). [15]

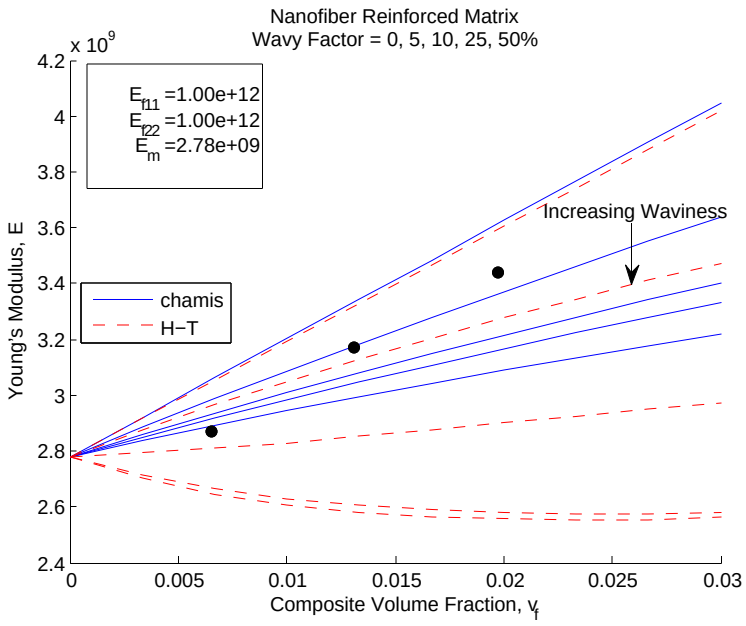

FIGURE 4.5. Zhou et al. experimental data (2.00/min strain rate). [15]

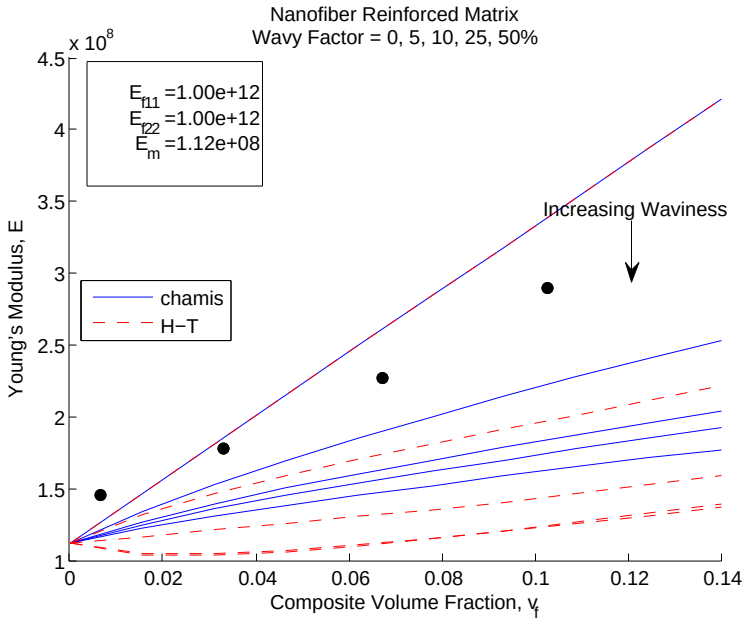

FIGURE 4.6. Ogale et al. experimental data. [45]

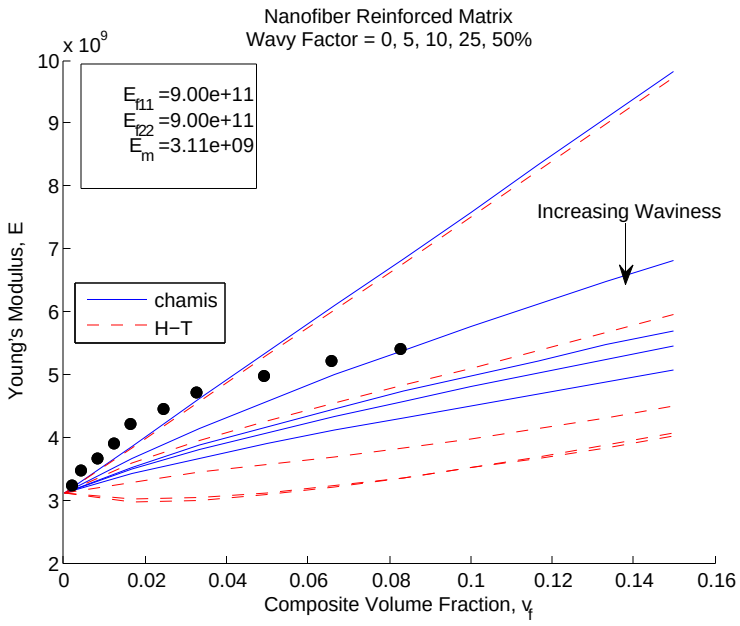

FIGURE 4.7. Omidi et al. experimental data. [33]

4.2 Three-Phase Composites

Relatively little experimental work has been published regarding three-phase composites. Yokozeki et al. [14] was the only article reviewed which prepared three-phase composites using unidirectional fibers. Carbon fiber prepregs were developed using resin infused with 5 and 10% by weight cup-stacked carbon nanotubes. Cup-stacked nanotubes are a special form of the MWNT, where each layer has been rolled up into a conical shape rather than a tube, as depicted in Figure 4.8. Unidirectional and quasi-isotropic laminates were fabricated and tested.

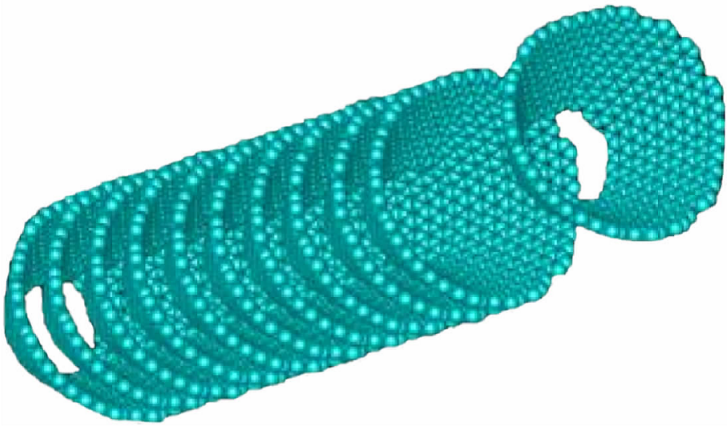

FIGURE 4.8. Cup stacked carbon nanotube. [46]

Since unidirectional fibers were used, the laminates can be analyzed using the current micromechanical model in combination with classical laminated plate theory. T700SC-12K fibers were used in combination with EP827 epoxy (Japan Epoxy Resin Co.) for the prepreg material. Detailed material data for these constituents was not readily available. T-300 Carbon Fiber (Table 4.1) and HY6010 epoxy (Table 4.2) properties were substituted for analysis, and comparisons between experiment and theory can be drawn by examining the *relative change* in properties over the baseline 0% laminate. Tables 4.3 and 4.5 show experimental three-phase results. Tables 4.4 and 4.6 show predictions from CLPT and both micromechanical models. Fiber volume fraction for each laminate was nominally 65% with a ply thickness of $0.125mm$. A waviness value of 10% was assumed for nanotubes.

Regarding the unidirectional laminate, experimental on-axis stiffnesses between the neat and CNF reinforced composite were statistically identical (standard deviation of 2.0 for tensile measurements). Both micromechanical models predict negligible increases in tensile stiffness. These results are expected because on-axis properties are dominated by the microfiber in the composite.

TABLE 4.1. T-300 Carbon Fiber Material Data [37]

Tensile E_{1f}	Transverse E_{2f}	Axial Shear G_{12f}	Transverse Shear G_{23f}	Poisson Ratio ν_{12f}
230 GPa	15 GPa	27 GPa	7 GPa	0.20

Transverse experimental stiffness showed an appreciable increase of almost 6% over the baseline. The Chamis implementation over-predicted this result at 8.5% over neat values. Experimental results showed good agreement with the Chamis model having waviness values between 5-25%, so using 10% here may be an underestimation. Conversely, the Halpin-Tsai implementation showed better agreement with experiment, albeit under-predicting results slightly.

Quasi-isotropic laminate results had a different behavior than did unidirectional. First, both A-G models under-predicted stiffness for the the 5 and 10% CNF weight loadings. The largest discrepancy is seen with the 5% case, where Halpin-Tsai and Chamis predicted 0.9% and 1.9% respective increases over baseline stiffness, but experimental results showed an increase of 3%. CNTs could be doing more than just making the matrix material stiffer. If they are improving the transfer of stress from the matrix to the microfibers it could result in a higher composite modulus, which wouldn't be captured by either of the presented micromechanical models.

It is interesting to note that doubling the weight fraction of nanotubes from 5 to 10% (which in this case is roughly equivalent to doubling volume fraction) in experiment resulted in only an additional 0.9% increase of stiffness. This could suggest that loading and stiffness in the 0-10% loading range have a non-linear relationship. Figure 2.13 had the largest experimental data set for two-phase composites and exhibits just such a non-linear response in this region.

TABLE 4.2. HY6010 Epoxy Material Data [37]

Young's Modulus, E_m	Poisson's Ratio, ν_m	Density, ρ_m
3.7 GPa	0.36	1.17 g/cm^3

TABLE 4.3. Three-Phase Composite Experimental Results (GPa), $[0]_{16}$ Unidirectional Laminate

Source	0% Weight		5% Weight	
	0° Stiffness	90° Stiffness	0° Stiffness	90° Stiffness
Experiment [14]	131	8.61	129 (-1.5%)	9.11 (+5.8%)

TABLE 4.4. Three-Phase Composite Theoretical Results (GPa), $[0]_{16}$ Unidirectional Laminate

Source	0% Weight		5% Weight	
	0° Stiffness	90° Stiffness	0° Stiffness	90° Stiffness
A-G (Chamis) + CLPT	150.7	8.793	151.0 (—)	9.537 (+8.5%)
A-G(Halpin-Tsai) + CLPT	150.7	8.793	150.8 (—)	9.143 (+4.0%)

TABLE 4.5. Three-Phase Composite Experimental Results (GPa), $[0/90/\pm 45]_{3s}$ Quasi-Isotropic Laminate

Source	0% Weight	5% Weight	10% Weight
Experiment [14]	46.5	47.9 (+3.0%)	48.3 (+3.9%)

TABLE 4.6. Three-Phase Composite Theoretical Results (GPa), $[0/90/\pm 45]_{3s}$ Quasi-Isotropic Laminate

Source	0% Weight	5% Weight	10% Weight
A-G (Chamis) + CLPT	57.8	58.9 (+1.9%)	59.7 (+3.3%)
A-G(Halpin-Tsai) + CLPT	57.8	58.3 (+0.9%)	58.7 (+1.6%)

CHAPTER 5

CONCLUSIONS AND FUTURE WORK

In this work, an existing micromechanical model (Anumandla-Gibson) for analysis of carbon nanotube reinforced composites was examined and subsequently implemented in MATLAB. It was then modified by replacing it's usage of the Chamis equations with that of the Halpin-Tsai equations since they are known to yield good approximations at low volume fractions. The model was then extended to three-phase composites using classical laminated plate theory.

Two-phase predictions showed promising results when compared with experimental results from literature. Waviness values between 0 and 25% for the Chamis model and 0 and 10% for the Halpin-Tsai model agree best with experiment. Three-phase results tended to under-predict improvement with nanotube loading, suggesting that another mechanism is at play besides a stiffer matrix.

One of the severely limiting aspects of experimental results thus far is a rigorous definition of geometry used. As was shown, this geometry determines key properties of the nanotube. This presents an issue because unlike microfibers which have relatively consistent geometry, nanotube lengths, diameters, and thicknesses are not be single valued due to how they are manufactured. Fisher et al. [16] used a *distribution* of waviness values in their micromechanical analyses. Along that same line, a model can be developed which takes a distribution of geometries into account. This would bring the analysis closer to reflecting reality. It would also allow direct correlation to experimental tests, where geometries and waviness could be identified through SEM or TEM imaging using a representative sample.

APPENDIX

EXPERIMENTAL DATA FROM LITERATURE

APPENDIX

EXPERIMENTAL DATA FROM LITERATURE

Most experimental results from literature reported data in terms of weight fractions, save for Andrews et al. (Table A.1, [43]) and Iwahori et al. (Table A.2, [44]). When conversion to volume fraction had to be made, the following was assumed:

- Matrix Density $\rho_m = 1.3g/cm^3$
- Fiber Density $\rho_f = 2.0g/cm^3$

Omidi et al. [33] provided a nanotube modulus $E_{NT} = 900GPa$. Referring to figures 2.5 and 2.6, this modulus corresponds to a density of about $\rho_f = 1.6g/cm^3$ which was used instead of the above $\rho_f = 2.0g/cm^3$. Volume fraction conversions were made using the following equation:

$$v_f = \frac{W_f/\rho_f}{W_f/\rho_f + (1 - W_f)/\rho_m}$$

where W_f is the weight fraction of the fiber.

TABLE A.1. Andrews Experimental Data [43]

$E_f = 1.0TPa$ (Assumed)
$E_m = 1.9GPa$

Volume Fraction,v_f	Composite Modulus, E_c (GPa)
0.05	2.2
0.1	3.05
0.15	3.85
0.25	4.55

TABLE A.2. Iwahori Experimental Data [44]

$E_f = 1.4TPa$
$E_m = 2.479GPa$

Weight Fraction, w_f	Volume Fraction, v_f	Composite Modulus, E_c (GPa)
0.05	0.021	2.826
0.10	0.041	3.628
0.05	0.021	2.636
0.10	0.41	3.602

TABLE A.3. Zhou Experimental Data (0.02/min strain rate) [15]

$E_f = 1.0TPa$ (Assumed)
$E_m = 2.31GPa$

Weight Fraction, w_f	Volume Fraction, v_f	Composite Modulus, E_c (GPa)
0.01	0.0065	2.39
0.02	0.0131	2.63
0.03	0.0197	2.84

TABLE A.4. Zhou Experimental Data (0.20/min strain rate) [15]

$E_f = 1.0TPa$ (Assumed)
$E_m = 2.49GPa$

Weight Fraction, w_f	Volume Fraction, v_f	Composite Modulus, E_c (GPa)
0.01	0.0065	2.64
0.02	0.0131	2.89
0.03	0.0197	3.03

TABLE A.5. Zhou Experimental Data (2.00/min strain rate) [15]

$E_f = 1.0TPa$ (Assumed)
$E_m = 2.78GPa$

Weight Fraction, w_f	Volume Fraction, v_f	Composite Modulus, E_c (GPa)
0.01	0.0065	2.87
0.02	0.0131	3.17
0.03	0.0197	3.44

TABLE A.6. Ogale Experimental Data [45]

$E_f = 1.0TPa$ (Assumed)
$E_m = 0.112GPa$

Weight Fraction, w_f	Volume Fraction, v_f	Composite Modulus, E_c (GPa)
0.01	0.0065	0.145
0.05	0.0331	0.178
0.10	0.0674	0.227
0.15	0.1029	0.29

TABLE A.7. Omidi Experimental Data [33]

$E_f = 0.9TPa$
$E_m = 3.11GPa$

Weight Fraction, w_f	Volume Fraction, v_f	Composite Modulus, E_c (GPa)
0.0025	0.0020	3.23
0.0050	0.0041	3.48
0.010	0.0081	3.67
0.015	0.0122	3.89
0.020	0.0163	4.20
0.030	0.0245	4.45
0.040	0.0327	4.70
0.060	0.0493	4.98
0.080	0.0660	5.22
0.100	0.0828	5.41

REFERENCES

REFERENCES

[1] Thostenson, E. T., and Chou, T.-W., 2003. "On the elastic properties of carbon nanotube-based composites: modelling and characterization". Journal of Physics D: Applied Physics, **36**(5), p. 573.

[2] Kis, A., and Zettl, A., 2008. "Nanomechanics of carbon nanotubes". Philosophical Transactions of the Royal Society of London A: Mathematical, Physical and Engineering Sciences, **366**(1870), pp. 1591–1611.

[3] Pipes, R. B., Frankland, S. J. V., Hubert, P., and Saether, E., 2002. "Self-consistent physical properties of carbon nanotubes in composite materials". NASA Langley Research Center, Hampton, VA NASA/CR-2002-212134.

[4] Gao, X.-L., and Li, K., 2005. "A shear-lag model for carbon nanotube-reinforced polymer composites". International Journal of Solids and Structures, **42**(5), pp. 1649–1667.

[5] Thostenson, E. T., Li, W. Z., Wang, D. Z., Ren, Z. F., and Chou, T. W., 2002. "Carbon nanotube/carbon fiber hybrid multiscale composites". Journal of Applied physics, **91**(9), pp. 6034–6037.

[6] Lourie, O., and Wagner, H. D., 1998. "Evaluation of Young's modulus of carbon nanotubes by micro-Raman spectroscopy". Journal of Materials Research, **13**(09), pp. 2418–2422.

[7] Sanchez-Portal, D., Artacho, E., Soler, J. M., Rubio, A., and Ordejn, P., 1999. "Ab initio structural, elastic, and vibrational properties of carbon nanotubes". Physical Review B, **59**(19), p. 12678.

[8] Yakobson, B. I., and Avouris, P., 2001. "Mechanical properties of carbon nanotubes". In Carbon nanotubes. Springer, pp. 287–327.

[9] Dresselhaus, M. S., Dresselhaus, G., and Saito, R., 1995. "Physics of carbon nanotubes". Carbon, **33**(7), pp. 883–891.

[10] Qian, H., Greenhalgh, E. S., Shaffer, M. S., and Bismarck, A., 2010. "Carbon nanotube-based hierarchical composites: a review". Journal of Materials Chemistry, **20**(23), pp. 4751–4762.

[11] Tehrani, M., Boroujeni, A. Y., Hartman, T. B., Haugh, T. P., Case, S. W., and Al-Haik, M. S., 2013. "Mechanical characterization and impact damage assessment of a woven carbon fiber reinforced carbon nanotubeepoxy composite". Composites Science and Technology, **75**, pp. 42–48.

[12] Boroujeni, A. Y., Tehrani, M., Nelson, A. J., and Al-Haik, M., 2014. "Hybrid carbon nanotubecarbon fiber composites with improved in-plane mechanical properties". Composites Part B: Engineering, **66**, pp. 475–483.

[13] Kanagaraj, S., Varanda, F. R., Zhiltsova, T. V., Oliveira, M. S., and Simes, J. A., 2007. "Mechanical properties of high density polyethylene/carbon nanotube composites". Composites Science and Technology, **67**(15), pp. 3071–3077.

[14] Yokozeki, T., Iwahori, Y., Ishiwata, S., and Enomoto, K., 2007. "Mechanical properties of CFRP laminates manufactured from unidirectional prepregs using CSCNT-dispersed epoxy". Composites Part A: Applied Science and Manufacturing, **38**(10), pp. 2121–2130.

[15] Zhou, Y., Jeelani, S., and Lacy, T., 2013. "Experimental study on the mechanical behavior of carbon/epoxy composites with a carbon nanofiber-modified matrix". Journal of Composite Materials, p. 0021998313512348.

[16] Fisher, F. T., Bradshaw, R. D., and Brinson, L. C., 2002. "Effects of nanotube waviness on the modulus of nanotube-reinforced polymers". Applied Physics Letters, **80**(24), pp. 4647–4649.

[17] Griebel, M., and Hamaekers, J., 2004. "Molecular dynamics simulations of the elastic moduli of polymercarbon nanotube composites". Computer methods in applied mechanics and engineering, **193**(17), pp. 1773–1788.

[18] Coleman, J. N., Khan, U., Blau, W. J., and Gunko, Y. K., 2006. "Small but strong: a review of the mechanical properties of carbon nanotubepolymer composites". Carbon, **44**(9), pp. 1624–1652.

[19] Fiedler, B., Gojny, F. H., Wichmann, M. H., Nolte, M. C., and Schulte, K., 2006. "Fundamental aspects of nano-reinforced composites". Composites science and technology, **66**(16), pp. 3115–3125.

[20] Saether, E., Frankland, S. J. V., and Pipes, R. B., 2003. "Transverse mechanical properties of single-walled carbon nanotube crystals. Part I: determination of elastic moduli". Composites Science and Technology, **63**(11), pp. 1543–1550.

[21] Shi, D.-L., Feng, X.-Q., Huang, Y. Y., Hwang, K.-C., and Gao, H., 2004. "The effect of nanotube waviness and agglomeration on the elastic property of carbon nanotube-reinforced composites". Journal of Engineering Materials and Technology, **126**(3), pp. 250–257.

[22] Mora, R. J., Vilatela, J. J., and Windle, A. H., 2009. "Properties of composites of carbon nanotube fibres". Composites Science and Technology, **69**(10), pp. 1558–1563.

[23] Anumandla, V., and Gibson, R. F., 2006. "A comprehensive closed form micromechanics model for estimating the elastic modulus of nanotube-reinforced composites". Composites Part A: Applied Science and Manufacturing, **37**(12), pp. 2178–2185.

[24] Shao, L. H., Luo, R. Y., Bai, S. L., and Wang, J., 2009. "Prediction of effective moduli of carbon nanotubereinforced composites with waviness and debonding". Composite structures, **87**(3), pp. 274–281.

[25] Yanase, K., Moriyama, S., and Ju, J. W., 2013. "Effects of CNT waviness on the effective elastic responses of CNT-reinforced polymer composites". Acta Mechanica, **224**(7), pp. 1351–1364.

[26] Odegard, G. M., Gates, T. S., Wise, K. E., Park, C., and Siochi, E. J., 2003. "Constitutive modeling of nanotubereinforced polymer composites". Composites science and technology, **63**(11), pp. 1671–1687.

[27] Chen, X. L., and Liu, Y. J., 2004. "Square representative volume elements for evaluating the effective material properties of carbon nanotube-based composites". Computational Materials Science, **29**(1), pp. 1–11.

[28] Seidel, G. D., and Lagoudas, D. C., 2006. "Micromechanical analysis of the effective elastic properties of carbon nanotube reinforced composites". Mechanics of Materials, **38**(8), pp. 884–907.

[29] Qian, D., Dickey, E. C., Andrews, R., and Rantell, T., 2000. "Load transfer and deformation mechanisms in carbon nanotube-polystyrene composites". Applied physics letters, **76**(20), pp. 2868–2870.

[30] Jones, R. M., 1975. Mechanics of composite materials, Vol. 1. McGraw-Hill New York.

[31] Liu, Y. J., and Chen, X. L., 2003. "Evaluations of the effective material properties of carbon nanotube-based composites using a nanoscale representative volume element". Mechanics of materials, **35**(1), pp. 69–81.

[32] Frankland, S. J. V., Harik, V. M., Odegard, G. M., Brenner, D. W., and Gates, T. S., 2003. "The stressstrain behavior of polymernanotube composites from molecular dynamics simulation". Composites Science and Technology, **63**(11), pp. 1655–1661.

[33] Omidi, M., DT, H. R., Milani, A. S., Seethaler, R. J., and Arasteh, R., 2010. "Prediction of the mechanical characteristics of multi-walled carbon nanotube/epoxy composites using a new form of the rule of mixtures". Carbon, **48**(11), pp. 3218–3228.

[34] Halpin, J. C., and Kardos, J. L., 1976. "The Halpin-Tsai equations: a review". Polymer engineering and science, **16**(5), pp. 344–352.

[35] Hsiao, H. M., and Daniel, I. M., 1996. "Elastic properties of composites with fiber waviness". Composites Part A: Applied Science and Manufacturing, **27**(10), pp. 931–941.

[36] Chamis, C. C., 1984. "Simplified composite micromechanics equations of hygral, thermal, and mechanical properties". Sampe Quarterly, **15**, pp. 14–23.

[37] Daniel, I. M., and Ishai, O., 1994. Engineering mechanics of composite materials, Vol. 3. Oxford university press New York.

[38] Christensen, R. M., and Waals, F. M., 1972. "Effective stiffness of randomly oriented fibre composites". Journal of Composite Materials, **6**(3), pp. 518–535.

[39] Halpin, J. C., 1969. Effects of Environmental Factors on Composite Materials. Tech. rep., DTIC Document.

[40] Ghavamian, A., Rahmandoust, M., and chsner, A., 2013. "On the determination of the shear modulus of carbon nanotubes". Composites Part B: Engineering, **44**(1), pp. 52–59.

[41] Nettles, A. T., 1994. Basic mechanics of laminated composite plates. Marshall Space Flight Center, National Aeronautics and Space Administration.

[42] Gibson, R. F., 2011. Principles of composite material mechanics. CRC press.

[43] Andrews, R., Jacques, D., Minot, M., and Rantell, T., 2002. "Fabrication of carbon multiwall nanotube/polymer composites by shear mixing". Macromolecular Materials and Engineering, **287**(6), pp. 395–403.

[44] Iwahori, Y., Ishiwata, S., Sumizawa, T., and Ishikawa, T., 2005. "Mechanical properties improvements in two-phase and three-phase composites using carbon nano-fiber dispersed resin". Composites Part A: Applied Science and Manufacturing, **36**(10), pp. 1430–1439.

[45] Ogale, A., Lee, S., and Kim, M.-S., 2010. "Influence of carbon nanofiber structure on polyethylene nanocomposites". Plastics Research Online.

[46] Yokozeki, T., Aoki, T., Arai, A., Ishibashi, M., and Yanagisawa, T., 2009. "Fabrication of CNT-dispersed CFRP using length-controlled CNTs: measurement of CNT length and characterization of mechanical properties". Tsinghua Science & Technology, **14**, pp. 100–104.